Toughened and Stiffened Nanocomposites Based on an Amorphous Polyamide Modified with Both Styrene/Ethylene-*co*-Butylene/Styrene Triblock Copolymer and an Organoclay

Imanol González, Asier Zabaleta, José I. Eguiazábal

Departamento de Ciencia y Tecnología de Polímeros and Instituto de Materiales Poliméricos "POLYMAT" Facultad de Ciencias Químicas UPV/EHU, San Sebastian, Spain

Received 11 February 2011; accepted 1 June 2011
DOI 10.1002/app.35031
Published online 11 October 2011 in Wiley Online Library (wileyonlinelibrary.com).

ABSTRACT: Polymer nanocomposites (PNs) based on an amorphous polyamide (aPA) modified with both a maleated rubber (mSEBS) for toughening, and with an organically modified organoclay for stiffening were obtained in the melt state. The PNs were highly dispersed and the organoclay was exclusively located in the aPA matrix. However, they showed a fine particle size that was larger than that of the corresponding blends. This indicates a lower compatibilization in the PNs that was attributed to a slight surfactant migration to the matrix during processing in the melt state. The increases in the modulus of elasticity upon organoclay (OMMT) addition were high enough to counteract the modulus decrease inherent to a 15% rubber addition. This allowed us to obtain a toughened aPA with a modulus similar to that of the unmodified aPA. The critical interparticle distance was lower in the PNs than in the corresponding blends. This decrease was attributed to the higher modulus of elasticity of the PNs matrix. © 2011 Wiley Periodicals, Inc. J Appl Polym Sci 124: 935–942, 2012

Key words: mechanical properties; nanocomposites; polyamides; toughness

INTRODUCTION

The interest in polymer nanocomposites containing nanoscale particles has spread from being mostly scientific towards being a clearly applied one. This is due to previous research efforts that have achieved large-scale exfoliation in many polymeric matrices that are attractive from a technological standpoint. Exfoliation allows a remarkable improvement in the properties of the matrix, such as thermal stability and mechanical performance, with very low filler contents thanks to the high surface area of the nanometric particles. However, despite the improvement in many desirable properties that a wide dispersion allows, the applications of the polymer nanocomposites are still limited by an imbalanced mechanical behavior, which is due to the very low levels of toughness that are commonly observed.

It is well known that in the case of notch sensitive thermoplastic matrices, rubber modification leads to large values of toughness at the expense of stiffness.[1–3] To improve compatibility and to achieve the fine particle size required (typically below 1 μm), compatibilization is often necessary.[1–3] Chemical modification of the rubber with maleic anhydride (MAH), for instance, is the most widely used technique.

Polyamides, both semicrystalline[2,4,5] and amorphous,[6–9] are a family of engineering polymers of great interest as matrices for toughened blends. Nanocomposites based on semicrystalline[10–13] and amorphous[14] polyamides have also been studied. These two facts have led researchers to fabricate nanocomposites based on these blends with the clear aim of moderating the stiffness decrease caused by the presence of rubber.

Several studies have been conducted on aPA matrices modified with both rubber[15] and organoclays. It has been shown that the addition of only a 15% of mSEBS caused an impressive 27-fold increase in the notched impact strength of the aPA, which, however, was accompanied by a notable decrease of the Young's modulus (20%).[15] Variations in the chemical nature of the amorphous polyamides can lead to different levels of organoclay dispersion, and also to different toughening levels, which can also be modified by the organoclay presence.[14,16] Several questions are, however, far from being fully understood.

Correspondence to: J. I. Eguiazábal (josei.eguiazabal@ehu.es).

Contract grant sponsor: Ministerio de Ciencia e Innovación; contract grant number: MAT2007-60153.

These are, for instance, the possibility of obtaining toughened nanocomposites, the influence of the organoclay presence on the brittle/tough transition, and the possible interaction between the rubber and the organoclay. Among the aPA-based PNs, the 4,4′-diamino-3,3′-dimethyldicyclohexylmethane-laurolactam-isophthalic acid copolymer has not been, to our knowledge, studied up to date. For this reason we have studied (i) whether toughening is possible in this aPA based nanocomposite, (ii) the effect of the OMMT on the morphological position of the brittle/tough (B/T) transition by means of the interparticle distance, and (iii) the parameters that influence the position of the B/T transition.

With these aims, a partially exfoliated aPA/OMMT PN with 3% OMMT was mixed with maleinized styrene/ethylene-butylene/styrene triblock copolymer (mSEBS) in the melt state. The nanostructure and microstructure of the PNs was characterized by X-ray diffraction (XRD), transmission electron microscopy (TEM) and scanning electron microscopy (SEM). The structure of the blends was studied by dynamic mechanical analysis (DMA), and their mechanical properties by means of tensile and notched Izod tests. A comparison between the position of the B/T transition in the PNs and in the blends will allow us to discuss the parameters on which the *B/T* transition depends on.

EXPERIMENTAL

The amorphous polyamide (aPA) used in this work was Grilamid® TR55 (EMS-Grivory), and the styrene/ethylene-butylene/styrene (SEBS) triblock copolymers were Kraton® G 1652 unmaleated and G 1901X maleated SEBS. The filler was a bis-2-hydroxyethyl tallow quaternary ammonium modified clay (Cloisite® 30B, Southern Clay Products) (OMMT). Commercial SEBS and maleic anhydride functionalized SEBS, were mixed to obtain the desired 1 wt % maleated SEBS (mSEBS). The mSEBS content in the PNs varied from 0 to 30 wt %. The PNs will be named by their mSEBS content; i.e., 20%-PN indicates a 80/20-3 aPA/mSEBS-OMMT PN. The materials designations and the compositions of the blends and PNs are summarized in Table I.

Drying before processing was performed at 100°C *in vaccuo* for 16 h for aPA, the two SEBS at 80°C in an air-circulation oven for 12 h, and in the case of the OMMT at 80°C in an air-circulation oven for 4 h. The a PA/OMMT nanocomposite matrix with 3 wt % OMMT was obtained using a Collin ZK25 corotating twin screw extruder-kneader. The diameter and length to diameter ratio of the screws were 25 mm and 30, respectively. The barrel temperature was 250°C and the rotation speed 200 rpm. Subsequently, the aPA/mSEBS-OMMT nanocomposites (PNs), and the reference aPA/mSEBS blends were obtained at a barrel temperature of 250°C and at a rotation speed of 100 rpm.

After extrusion, the extrudate was cooled in a water bath and pelletized. Subsequent injection molding was carried out in a Battenfeld BA230E reciprocating screw injection molding machine to obtain tensile (ASTM D638, Type IV, thickness 3.2 mm) and impact (ASTM D256, thickness 3.1 mm) specimens. The screw of the plasticization unit had a diameter of 18 mm, *L/D* ratio of 17.8 and compression ratio of 4. The melt temperature was 250°C and the mould temperature was held at 15°C. The injection speed and pressure 13.5 cm^3/s and 1870 bar, respectively.

Capillary rheometry measurements were performed at 250°C in a Göttfert Rheograph 2002 extrusion rheometer using a flat entry capillary tungsten die with an *L/D* ratio of 30/1. The phase structure of the PNs was studied by DMA analysis performed using a TA Q800 that provided the loss tangent (tan δ) against temperature. The scans were carried out in bending mode at a constant heating rate of 4°C/min and a frequency of 1 Hz from –100 to 200°C. X-ray diffraction patterns were recorded in a Philips PW 1729 GXRD X-ray diffractometer at 45 kV and 50 mA, using Ni-filtered Cu-Kα radiation source. The scan speed was 0.5°/min. The transmission electron microscopy (TEM) samples were ultrathin-sectioned at 60–100 nm using an ultramicrotome. The micrographs were obtained in a Philips CM200 apparatus at an accelerating voltage of 200 kV.

The surfaces of cryogenically fractured specimens were observed by SEM after gold coating. A Hitachi S-2700 electron microscope was used at an accelerating voltage of 15 kV. The cryogenically fractured surfaces were etched with toluene for 2 h to remove the mSEBS. The rubber particle size was measured in representative zones of the cryogenically fractured impact specimens. The weight average particle size, $\overline{d}_w$, was calculated from a minimum of 200 particles as follows:

$$\overline{d}_w = \frac{\sum_i n_i d_i^2}{\sum_i n_i d_i}, \quad (1)$$

where n_i is the number of particles with size d_i. The inter-particle distance (τ) was calculated by means of:

$$\tau = \overline{d}_w \left[\left(\frac{\pi}{6\phi} \right)^{1/3} - 1 \right] \quad (2)$$

where ϕ is the volume fraction of the matrix.

The tensile tests were carried out in an Instron 5569 tensile tester at a cross-head speed of 10 mm/min at 23 ± 2°C and 50 ± 5% relative humidity. The mechanical properties [tensile strength (σ_t) and

ductility, measured as the break strain (ε_b)] were determined from the load-displacement curves at a cross-head speed of 10 mm/min. The Young's modulus was determined by means of an extensometer at a cross-head speed of 1 mm/min. Izod impact tests were carried out on notched specimens using a Ceast 6548/000 pendulum. The notches (depth 2.54 mm and radius 0.25 mm) were machined after injection molding. A minimum of seven tensile specimens and eight impact specimens were tested for each reported value.

RESULTS AND DISCUSSION

Phase behavior

The phase behavior of the ternary PNs was studied by DMA. Figure 1 shows the tanδ against temperature plot of the 15 and 25% PNs, and respective blends, aPA/OMMT, pure aPA, and mSEBS as a reference. The glass transition temperatures (T_g) of all compositions are collected in Table II. As can be seen, the pure mSEBS showed two tan δ peaks at around −48°C and 100°C, which corresponds to ethylene-butylene and styrene phase, respectively. The low temperature T_g increased with the mSEBS content. This behavior is unusual in thermoplastic/rubber blends.[17–19] However, it was also observed in polyamide/mSEBS blends[2] and it was attributed to the presence of copolymers produced by the reaction between the terminal amine groups of the aPA and the MAH of mSEBS.

The high temperature T_g, which corresponds to the aPA phase (T_g: 163°C), decreased slightly with increasing mSEBS content. This decrease was small (∼ 2.5°C), and can be attributed to the presence of miscibilized copolymers. However, the decrease in the T_g of the PNs with respect to that of the corresponding blend (i.e., a possible OMMT effect) was approximately constant and close to 1°C. It has been shown that the high temperature T_g may decrease in the presence of OMMT due to migration and dissolution of some surfactant in the matrix.[20] Provided this migration occurred in our PNs, the observed T_g change should be small because the OMMT content of the PNs of this study is also low (3%). Consequently, an extremely small decrease in T_g due to some surfactant migration is possible and will be discussed in further detail below.

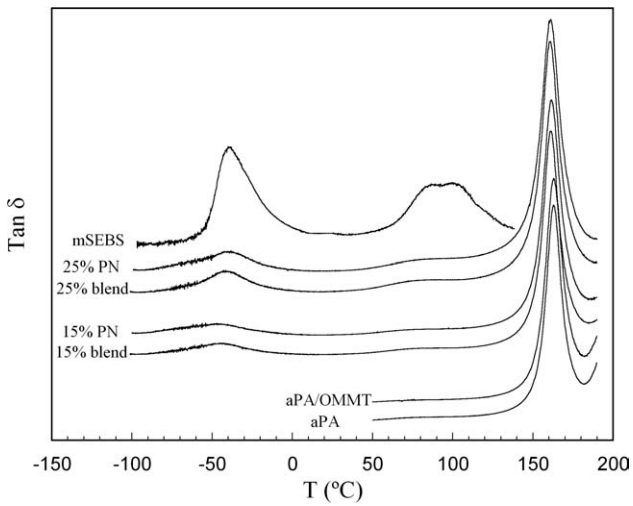

Figure 1 DMA plots of tanδ versus temperature for 15 and 25%-PNs, and respective blends, aPA/OMMT, pure aPA, and mSEBS as reference.

Characterization of the nanostructure

The characterization of the nanostructure of the ternary PNs was carried out by both XRD and TEM. The XRD plots of the 10% and 20%-PNs as well as that of the OMMT are shown in Figure 2. The OMMT shows a characteristic peak at 2θ: 4.85° (d_{001}: 1.88 nm). On the other hand, the scans of the PNs

TABLE I
Materials Designation

Materials designation	Composition
Grilamid® TR55	aPA
Kraton® G1652/Kraton® G1901X 50/50	mSEBS
aPA/OMMT	aPA/OMMT 97/3
5%-PN	aPA/mSEBS-OMMT 95/5-3
10%-PN	aPA/mSEBS-OMMT 90/10-3
15%-PN	aPA/mSEBS-OMMT 85/15-3
20%-PN	aPA/mSEBS-OMMT 80/20-3
25%-PN	aPA/mSEBS-OMMT 75/25-3
30%-PN	aPA/mSEBS-OMMT 70/30-3
5%-blend	aPA/mSEBS 95/5
10%-blend	aPA/mSEBS 90/10
15%-blend	aPA/mSEBS 85/15
20%-blend	aPA/mSEBS 80/20
25%-blend	aPA/mSEBS 75/25

TABLE II
Glass Transition Temperature (T_g) of PNs Versus mSEBS Content, and the aPA/mSEBS Blend and mSEBS as a Reference

mSEBS (%)	High temperature T_g (°C)	Low temperature T_g (°C)
0	163.1 ± 0.3	–
5	162.4 ± 0.3	−47.8 ± 0.2
10	162.4 ± 0.1	−47.4 ± 0.3
15	161.7 ± 0.3	−45.1 ± 0.7
20	161.5 ± 0.2	−42.7 ± 0.1
25	161.2 ± 0.1	−40.8 ± 0.1
30	160.7 ± 0.1	−39.2 ± 0.5
aPA/mSEBS	163.0 ± 0.3	−48.1 ± 0.2
mSEBS	–	−48.1 ± 0.2

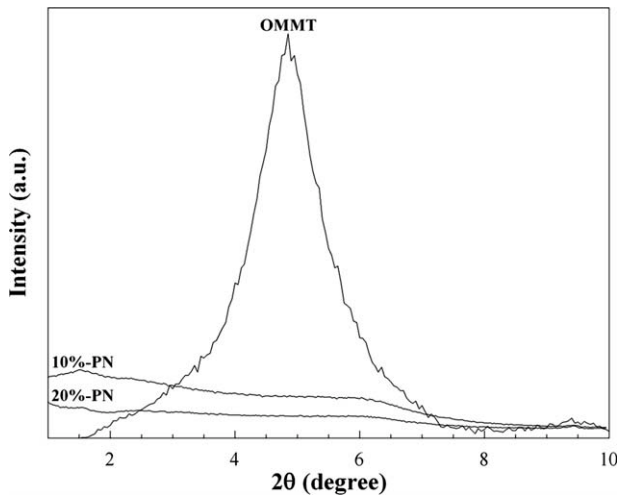

Figure 2 X-ray diffraction patterns for OMMT, 10 and 20%-PNs.

showed a small main peak at 2θ: 1.55° (d_{001}: 5.19 nm), indicating the presence of intercalated structures.

Figure 3(a,b) show TEM photomicrographs of the 20%-PN and the binary aPA/OMMT PN, respectively. Figure 3(a) shows that the clay layers stayed in the aPA matrix, and no preferential segregation of the clay to the interface occurred. The rubbery nature of the dispersed phase was maintained in the PNs, as the clay did not migrate to the rubber during melt mixing. In addition, dispersion was very high as most particles are constituted of a single clay layer. A comparison between Figure 3(a,b) showed that the dispersion level of both PNs is very similar. This indicates that the additional processing that the incorporation of mSEBS implies [Fig. 3(a)] did not lead to any compaction of the widely exfoliated layers.

Morphology

The morphology of the dispersed rubber phase of the 10 and 20%-PNs, and that of their corresponding reference blends, are shown in Figure 4(a–d), respectively. The rubber particle size data of all compositions is collected in Table III. Blending was effective in all compositions, although some coalesced particles were seen at high rubber contents. The dispersed rubber particle size in both the PNs and in the blends was observed to increase with increasing rubber content, as is expected for toughened thermoplastic blends.[1] This fine particle size both in PNs and blends is attributed to the higher viscosity of the aPA/OMMT and pure aPA matrices compared with that of mSEBS (the viscosity of the matrices at 250°C and a shear speed of 200 s^{-1} were 2620 and 2845 Pa s^{-1}, and that of mSEBS was 340 Pa s^{-1}), which makes mastication of the dispersed phase easier. In contrast with previous observations,[14] a comparison between the morphology of the PNs [Fig. 4(a,b)] and that of the reference blends [Fig. 4(c,d)], demonstrates that the particle size of the PNs was slightly larger than that of the corresponding blends (Table III).

To understand the reasons behind the particle size increase observed after OMMT addition (Fig. 4 and Table III), we examined the deformation and breaking, and therefore the particle size of the dispersed phase, in a polymer blend. The parameters that influence these processes are captured in the Capillary number,[21,22] which is the ratio of the viscous stress to deform the particle in a simple shear flow

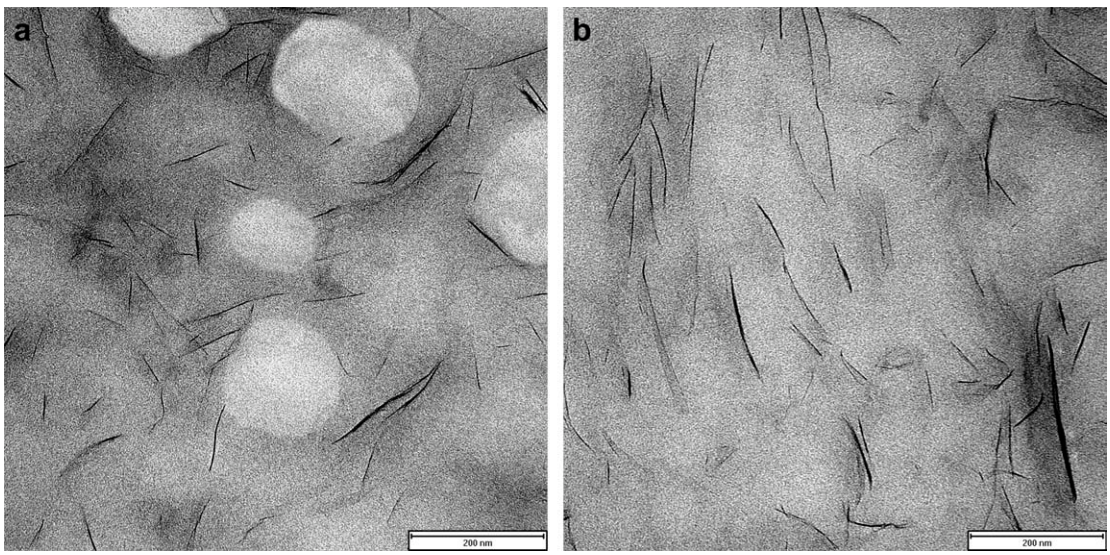

Figure 3 TEM photomicrographs of (a) 20%-PN and (b) aPA/OMMT.

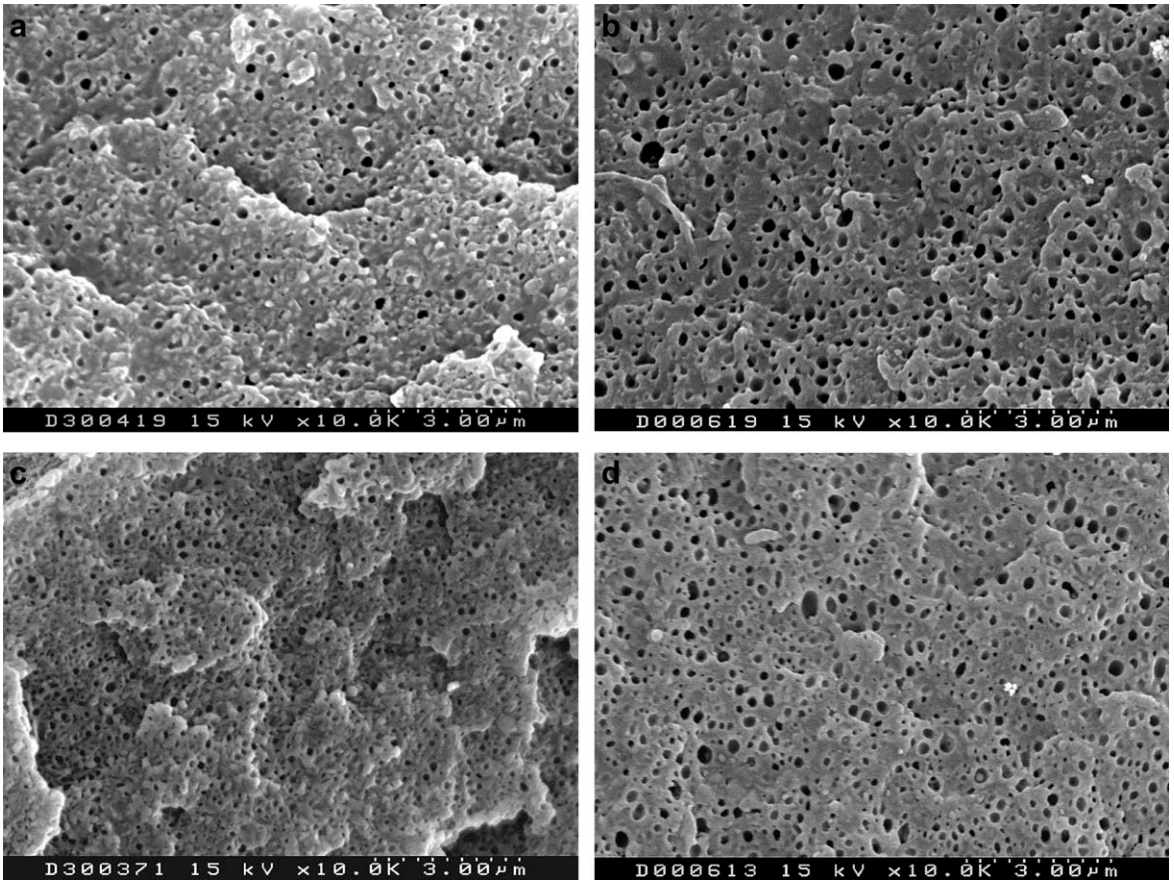

Figure 4 Cryofractured etched surfaces of the injection molded impact specimens of (a) 10%-PN, (b) 20%-PN, (c) 10%-blend, and (d) 20%-blend.

to the interfacial tension that tends to keep the particle spherical

$$C_a = \frac{\mu_m \dot{\gamma}}{\sigma/R}$$

where μ_m is the viscosity of the matrix, $\dot{\gamma}$ is the shear rate, σ the interfacial tension, and R the radius of the particle. For a capillary number higher than a critical value the particle breaks up. The critical C_a depends on the type of flow (shear or elongational) and on the viscosity ratio. In the PNs of this study, the change in particle size observed in Figure 4 should be due to variations in either the viscosity of the matrix or the interfacial tension, since processing conditions such as $\dot{\gamma}$ were the same for the reference blend and for the PNs. Other parameters not included in the Capillary number equation, such as a barrier effect of the inorganic particles hindering coalescence,[14] should lead to the opposite effect observed.

To test a possible effect of the viscosity of the matrix, the viscosity of the binary aPA/OMMT PN and that of pure aPA (which are the matrices of the PNs and of the blends, respectively) were measured using capillary rheometry, and the results are shown in Figure 5. The viscosity of the binary PN was very similar to that of the pure aPA, especially at higher shear rates (predominant in the extrusion process). This means that the viscosity of the matrix is not the reason for the larger particle size obtained in the PNs.

We then looked, at the dispersed particle/matrix interface in the PNs and in the blends to evaluate if the interfacial tension was the reason for the larger particle size (lower degree of compatibilization) of

TABLE III
Weight-Average Particle Size (d_w) of PNs and Blends at Different mSEBS Contents

mSEBS (wt %)	d_w (µm)	
	PNs	Blends
5	0.16	0.13
10	0.21	0.17
15	0.28	0.20
20	0.33	0.22
25	0.40	0.25
30	0.49	–

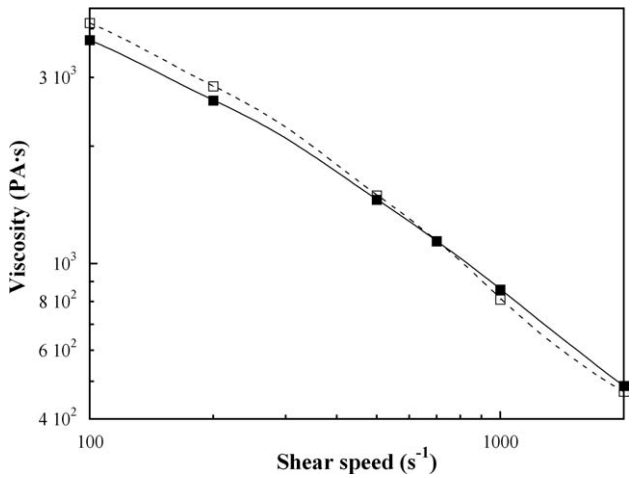

Figure 5 Apparent viscosity of the binary aPA/OMMT PN (■) and the pure aPA (□).

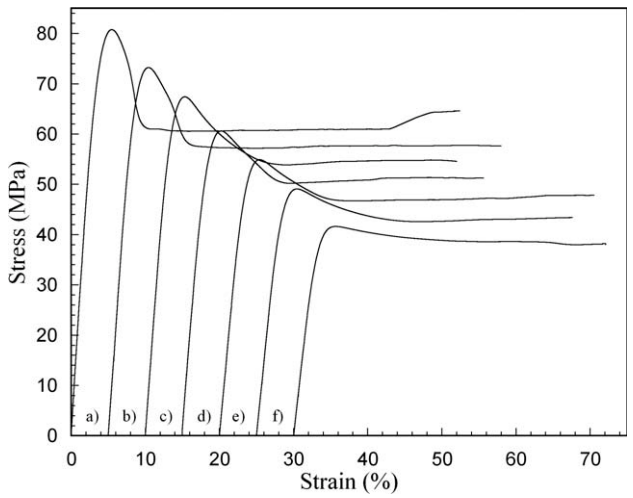

Figure 6 Tensile stress–strain curves of the (a) aPA/OMMT PN and (b) 5, (c) 10, (d) 15, (e) 20, (f) 25, and (g) 30%-PN. The curves are slipped in the X-axis for the sake of clarity.

the PNs. As was seen in Figure 3(a), the inorganic clay particles of the PNs were not located at the matrix/rubber interface and, therefore, they could not have modified the matrix/rubber interfacial tension. The surfactant of the clay, however, could have migrated during processing and dissolved in the matrix.[23,24] This could lead to interactions between the surfactant and the MAH groups of the mSEBS, thus blocking the maleic groups of mSEBS, and causing a decrease in the compatibilization ability of mSEBS.[11] The low contents of OMMT (and, therefore, surfactant content) present in our PNs should only result in a slight surfactant migration, which agrees with both the small, high temperature T_g decrease (see Table II) as well as with the small particle size increase observed. Therefore, we propose that the small particle size increase observed is due to a slight migration of surfactant, and its negative effect on compatibilization.

Mechanical properties

The mechanical properties of the PNs were studied by means of both tensile and impact tests. The tensile stress–strain curves of the PNs are shown in Figure 6. As can be seen, the matrix broke in the strain-hardening region. The PNs were ductile in all mSEBS range, showing a cold-drawing region where fracture occurred. Figure 7 shows the Young's modulus of the PNs and that of their corresponding blends as a function of the mSEBS content. The yield stress showed a similar behavior. As can be seen, the Young's modulus increased substantially with the addition of OMMT. The increase in modulus (28%) was similar to that obtained in other aPA based PNs[25–27] with the same clay content. The increases in both the modulus and the yield stress were for the most part independent of the mSEBS content, and therefore, their relative importance increased at increasing rubber contents. These modulus increases indicate a decrease in molecular mobility. The decrease in molecular mobility is enhanced by the large interfacial area to dispersed phase volume ratio characteristic of partially exfoliated PNs, and indicates the presence of strong interactions between the polymer chains and the silicate layers.

The modulus of the PNs decreased with the mSEBS content as a consequence of the elastomeric nature of the mSEBS. However, the fundamental effect of the OMMT presence is seen in Figure 7. That is, since the modulus of the 15%-PN was very similar to that of the pure aPA (Fig. 7), the 3% OMMT of this study was able to counteract the

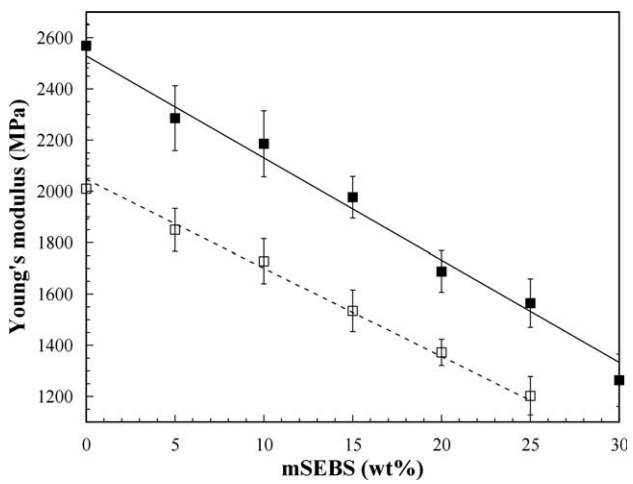

Figure 7 Young's modulus of the PNs (■) and blends (□) versus mSEBS content.

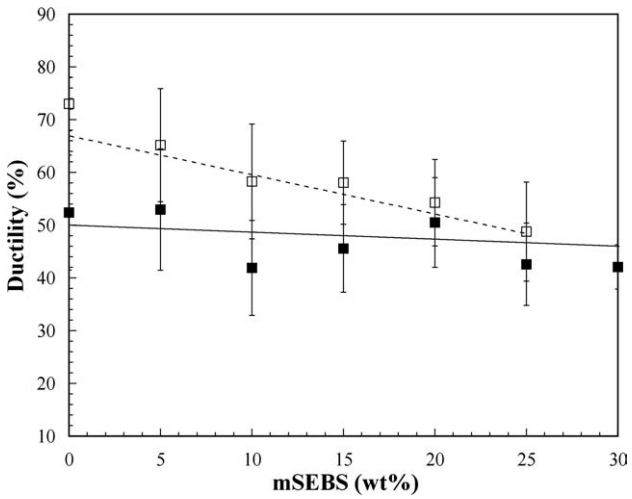

Figure 8 Ductility of the PNs (■) and blends (□) versus mSEBS content.

negative influence of almost 15% rubber on the modulus.

Figure 8 shows the ductility of both the PNs and their blends as a function of the mSEBS content. The addition of OMMT diminished the ductility of the blends due to constraints on the mobility of the chains caused by the partially exfoliated platelets. The incorporation of mSEBS to the PNs did not result in a decrease in ductility, as observed in the case of the blends. This is consistent with the presence of dissolved surfactant, which it is known[28] to behave as a plasticizer. All the PNs were ductile since they always broke during cold drawing.

The notched impact strength of the PNs, and that of the corresponding blends as a reference, is shown in Figure 9 as a function of the rubber content. The figure reveals a clear brittle/tough (B/T) transition in the impact strength of the 10 and 20%-PN, which results in an increase in toughness from 115 to 635 J/m. The highest impact strength value is typical of super-toughness (11-fold that of the aPA). It is also slightly higher than that of the aPA/mSEBS blends of this study (600 J/m), as well as higher than the value reported in the literature[15] for the same aPA. As stated before, the tough nature of the PNs is accompanied by modulus of elasticity values only slightly below that of the pure aPA matrix. Thus, the 20%-PN shows the best balance of properties, since this PN combines the stiffness of pure aPA with impact strength values 10-fold that of the matrix.

The high increase in toughness observed in the impact strength tests with mSEBS content was not observed in the case of elongation at break. This behavior must be attributed to the different mechanisms that involve the fracture both in the elongation at break (tensile test) and impact strength (Izod impact test), which are consequence of the different geometry and test speed used.

Nowadays, the study of the critical morphology leading to the brittle/tough transition is usually conducted in terms of a critical interparticle distance (τ_c)[29–31] (also named ligament thickness), rather than in terms of a critical particle size. The τ_c allows the stress conditions to change from plane strain to plane stress ones,[29] thus strongly modifying the deformation characteristics. For this reason, the τ_c of the PNs and that of their respective blends was measured and is shown as a function of the impact strength in Figure 10. As can be seen, the *B/T* transition of the PNs took place at roughly τ: 0.10 μm, while that of the blends appeared at approximately 0.13 μm. Thus, the addition of OMMT led to a decrease in τ_c.

It is known that τ_c depends on both extrinsic[30,32–36] and intrinsic[3,19,33,37,38] parameters; this makes it difficult to study the dependence of τ_c on each individual parameter. However, if we compare the τ_c of the

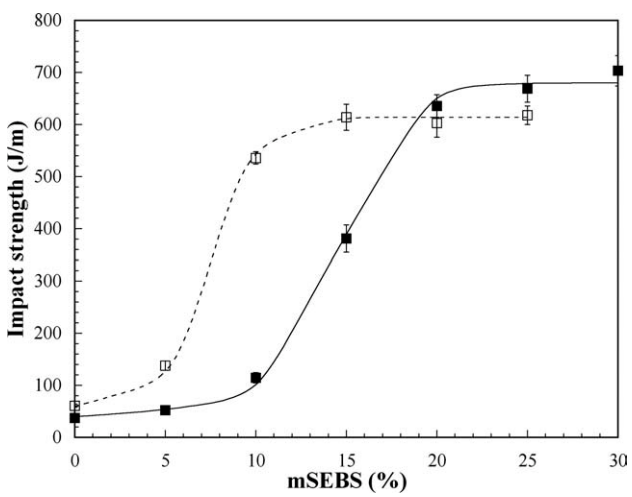

Figure 9 Notched impact strength of the PNs (■) and blends (□) versus mSEBS content.

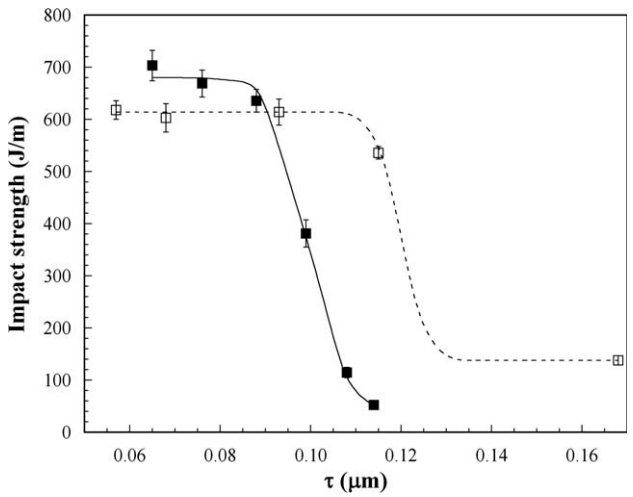

Figure 10 Notched impact strength of the PNs (■) and blends (□) versus interparticle distance (τ).

PNs with that of their respective blends, the extrinsic parameters (experimental conditions) will remain constant. Moreover, the intrinsic parameters related to the rubber and the compatibilizer are also expected to remain constant. Consequently, the observed change in τ_c has to be attributed to a change of either the interfacial adhesion or the modulus of elasticity of the matrix. The slightly lower interfacial adhesion of the PNs should lead to a smaller τ_c[10,39]; however, the opposite effect was observed.

The modulus of elasticity of the matrix changed from 2010 for the pure aPA to 2570 MPa for the binary PN. Consequently, in agreement with previous observations,[24] we propose that the modulus of elasticity is the main parameter responsible for the change in τ_c, wherein the higher modulus of the matrix of the PNs led to a lower τ_c.

CONCLUSIONS

The main result that can be extracted of this work is that we can obtain a tough nanocomposite based on aPA which combines the tough nature of elastomer with the stiffness of the clay.

The T_g of the aPA matrix decreased slightly upon OMMT addition. This fact, together with the decrease in compatibilization in the presence of OMMT, indicate that some surfactant migrated to the matrix and interacted with the MAH leading to a slightly larger particle size in the PNs compared to that of the corresponding blends.

XRD and TEM revealed a high degree of clay dispersion in the PNs characterized by a majority of monolayer particles, and which was shown to be independent of the rubber content. The particles remained only in the matrix; this preserved the rubbery nature of the dispersed phase and rules out any possible influence of the inorganic particles on the interfacial tension.

Because of the fact that the inorganic particles remained in the matrix and that there was no significant change in the viscosity of the matrix, we attributed the increase in particle size observed to a slight surfactant migration and its negative effect on the compatibilization of the blends.

A brittle/tough transition close to that of a 15% rubber was clearly observed in the PNs. Moreover, the 3% OMMT of this study was able to counteract the negative influence of almost 15% rubber content on the modulus. Thus, the OMMT addition is able to counteract the inherent weakness of toughened blends, i.e., their low modulus of elasticity, while preserving their tough nature.

The addition of OMMT led to a decrease in τ_c. This decrease in τ_c was ascribed primarily to the higher modulus of the matrix in the PNs.

Technical support of the Polymer Characterization Service of the University of Basque Country for the TEM and XRD analysis are gratefully acknowledged.

References

1. Paul, D. R.; Bucknall, C. B. Polymer Blends; Wiley: New York, 2000.
2. Oshinski, A. J.; Keskkula, H.; Paul, D. R. Polymer 1992, 33, 268.
3. Gaymans, R. J.; Borggreve, R. J. M.; Spoelstra, A. B. J Appl Polym Sci 1989, 37, 479.
4. Oshinski, A. J.; Keskkula, H.; Paul, D. R. Polymer 1996, 37, 4891.
5. Kayano, Y.; Keskkula, H.; Paul, D. R. Polymer 1997, 38, 1885.
6. Huang, J.; Paul, D. R. Polymer 2006, 47, 3505.
7. Huang, J. J.; Keskkula, H.; Paul, D. R. Polymer 2004, 45, 4203.
8. Huang, J. J.; Keskkula, H.; Paul, D. R. Polymer 2006, 47, 624.
9. Huang, J. J.; Keskkula, H.; Paul, D. R. Polymer 2006, 47, 639.
10. González, I.; Eguiazabal, J. I.; Nazabal, J. J Polym Sci Pol Phys 2005, 43, 3611.
11. Gonzalez, I.; Eguiazabal, J. I.; Nazabal, J. Eur Polym J 2006, 42, 2905.
12. Gonzalez, I.; Eguiazabal, J. I.; Nazabal, J. Compos Sci Technol 2006, 66, 1833.
13. Ahn, Y. C.; Paul, D. R. Polymer 2006, 47, 2830.
14. Yoo, Y.; Cui, L.; Yoon, P. J.; Paul, D. R. Macromolecules 2010, 43, 615.
15. Gonzalez, I.; Eguiazabal, J. I.; Nazabal, J. Polym Eng Sci 2009, 49, 1350.
16. Yoo, Y.; Tiwari, R. R.; Yoo, Y.-T.; Paul, D. R. Polymer 2010, 51, 4907.
17. Guerrica-Echevarria, G.; Eguiazabal, J. I.; Nazabal, J. Macromol Mater Eng 2005, 290, 38.
18. Arostegui, A.; Nazabal, J. Polym Eng Sci 2003, 43, 1691.
19. Arostegui, A.; Nazabal, J. Polym J 2003, 35, 56.
20. Zabaleta, A.; Gonzalez, I.; Eguiazabal, J. I.; Nazabal, J. Polym Eng Sci 2011, 51, 1428.
21. Zhang, B. Q.; Ding, Y. F.; Chen, P.; Liu, C. Y.; Zhang, J.; He, J. S.; Hu, G. H. Polymer 2005, 46, 5385.
22. Shariatpanahi, H.; Nazokdast, H.; Hemmati, M. J Appl Polym Sci 2003, 88, 54.
23. Gonzalez, I.; Eguiazabal, J. I.; Nazabal, J. Polym Eng Sci 2006, 46, 864.
24. Gonzalez, I.; Eguiazabal, J. I.; Nazabal, J. Eur Polym J 2008, 44, 287.
25. Goitisolo, I.; Eguiazabal, J. I.; Nazabal, J. Polym Adv Tech 2009, 20, 1060.
26. Yoo, Y.; Paul, D. R. Polymer 2008, 49, 3795.
27. Zhang, X.; Loo, L. S. J Polym Sci Polym Phys 2008, 46, 2605.
28. Morgan, A. B.; Harris, J. D. Polymer 2003, 44, 2313.
29. Wu, S. H. Polymer 1985, 26, 1855.
30. Jiang, W.; Liu, C. H.; Wang, Z. G.; An, L. J.; Liang, H. J.; Jiang, B. Z.; Wang, X. H.; Zhang, H. X. Polymer 1998, 39, 3285.
31. Borggreve, R. J. M.; Gaymans, R. J.; Eichenwald, H. M. Polymer 1989, 30, 78.
32. Borggreve, R. J. M.; Gaymans, R. J.; Schuijer, J.; Ingen Housz, J. F. Polymer 1987, 28, 1489.
33. Kanai, H.; Sullivan, V.; Auerbach, A. J Appl Polym Sci 1994, 53, 527.
34. Wu, S. J Appl Polym Sci 1988, 35, 549.
35. Dijkstra, K.; Terlaak, J.; Gaymans, R. J. Polymer 1994, 35, 315.
36. Jiang, W.; Tjong, S. C.; Li, R. K. Y. Polymer 2000, 41, 3479.
37. Arostegui, A.; Nazabal, J. Polymer 2003, 44, 239.
38. Arostegui, A.; Nazabal, J. J Polym Sci Polym Phys 2003, 41, 2236.
39. Liu, Z. H.; Zhu, X. G.; Wu, L. X.; Li, Y.; Qi, Z. N.; Choy, C.; Wang, F. S. Polymer 2001, 42, 737.